Imperial College London

ZSL LET'S WORK FOR WILDLIFE

The application of remote sensing to monitor loss of kelp habitat along the Sussex coastline

Alexander James August Briggs

August 2020

A thesis submitted for the partial fulfilment of the requirements for the degree of Master of Science at Imperial College London

Formatted in the journal style of Methods in Ecology and Evolution

Submitted for the MSc in Ecology, Evolution and Conservation

Declaration

No primary data collection was undertaken for this project. Zoological Society of London (ZSL) provided data quantifying anthropogenic fishing activity, based on data from Global Fishing Watch (2020). A dataset of processed imagery showing kelp distribution (used for ground truthing) was provided to me by ZSL, based on towed video transects. Additionally, ZSL provided raw video footage for additional transects, which I then analysed. I collated all other data used for this project from multiple sources. Through the biodiversity recording website National Biodiversity Network Atlas (2020), I collated observations of kelp distribution based on records taken by divers (Seasearch, 2019). I collated Sentinel satellite imagery from the Copernicus Open Access Hub (European Space Agency, 2020a). I collated weather and tidal data from the Chimet weather buoy and the weather forecasting and archival website Tides4Fishing (Chimet Support Group, 2020; Tides4Fishing, 2020). I sourced a Digital Elevation Model showing bathymetry, created by OceanWise, from the spatial data repository Edina Digimaps (OceanWise, 2016). I also sourced sediment data, created by British Geological Survey, from Edina Digimaps (British Geological Survey, 2011). Guidance and advice were provided by my internal and external supervisors, Dr. James Rosindell (Imperial College London) and Dr. Chris Yesson (Zoological Society of London). I carried out all data cleaning and analysis.

Acknowledgements

This project was significantly altered and limited by the national lockdown which took place during the Coronavirus pandemic. This prevented drone surveys and the collection of high-resolution remote sensing and ground truthing data, limiting the scope of this study. Therefore, for their assistance in overcoming these issues, I thank my supervisors, Dr. Rosindell and Dr. Yesson. I also thank my course-mates for their support and advice.

Word count: 5,997

Abstract

Kelp forests, one of the most biodiverse habitats on earth and holding a high ecosystem service value, are declining globally due to climate change and anthropogenic fishing activities. Despite these threats, kelp distributions are often unmonitored, preventing critical conservation action. In the UK, along the Sussex coastline, once abundant kelp forests have declined to functional absence. This thesis established a standardised remote sensing-based monitoring method for this study area, using satellite imagery. Three image classification methods commonly used to study kelp were evaluated. The most accurate, a supervised classification, was then applied to produce a species distribution model, predicting the distribution of over 100km^2 of kelp across Sussex. Kelp distribution was positively associated with fishing activity, suggesting that trawling may be linked with kelp decline in this area. However, low model accuracy suggests that these results should be treated with caution. This thesis highlights the limitations of widely available remote sensing data for monitoring sublittoral kelp in turbid waters. The collection of high-quality remote sensing data must be prioritised to monitor the distribution of declining kelp forests and inform conservation efforts.

1 Introduction

Habitat loss is a critical factor contributing to the current biodiversity crisis (Fahrig, 1997; Pardini, Nichols and Püttker, 2017). To protect biodiversity and ecosystem functioning, conservation must prevent habitat loss (Fahrig, 1997; Brooks *et al.*, 2002). The imperative to identify and halt the decline of threatened habitats is highlighted by the aims of the Red List of Ecosystems (International Union for Conservation of Nature, 2020), and the Convention on Biological Diversity (2018). Kelp forests, declining across their global distribution, exemplify habitat loss which threatens high levels of dependant biodiversity (Dayton *et al.*, 1992; Steneck *et al.*, 2002; Casal, Sánchez-Carnero, *et al.*, 2011).

Laminariales, known as kelp, are a diverse order of large brown macroalgae (Bolton, 2010). Various species of kelp form forest communities which dominate rocky, sublittoral zones on temperate coastlines (Dayton, 1985; Bolton, 2010). Having a high secondary productivity, kelp forests are some of the most biodiverse habitats on earth. Kelp communities provide nutrition for grazers and increase habitat complexity, supporting species of high ecological and commercial value such as the Atlantic cod (*Gadus morhua*; Steneck *et al.*, 2002; Smale *et al.*, 2013; Teagle *et al.*, 2017). Christie, Norderhaug and Fredriksen (2009) found, within kelp forests, faunal densities of over 100,000 individuals per m^2. Other regulating ecosystem services provided by kelp forests include carbon sequestration, wave attenuation, and water filtering (Steneck *et al.*, 2002). Kelp also provide provisioning ecosystem services as a fertiliser, fuel, and food source (Chung *et al.*, 2011; Mac Monagail *et al.*, 2017; FAO, 2018). Due to such high ecological and anthropogenic value, further research to ensure the sustainability of kelp communities is necessary (Mac Monagail *et al.*, 2017).

Kelp forests around the world are declining due to numerous threats including climate change and anthropogenic activities (Dayton *et al.*, 1992; Steneck *et al.*, 2002; Casal, Sánchez-Carnero, *et al.*, 2011). Due to the narrow thermal tolerance of many algal species, sea temperature plays a major role in determining species' range (Breeman, 1988). Brodie *et al*., (2014) suggests that due to climate change, southern Atlantic distributions of kelp will disappear. In addition, climate change will decrease carbon sequestration as kelp productivity is reduced at higher temperatures (Chung *et al.*, 2011; Pessarrodona *et al.*, 2018). Human activities, such as kelp harvesting, overfishing, and trawling, can also lead to the decline of kelp forests (Steneck *et al.*, 2002). Overfishing, in particular, facilitates the overgrazing of kelp by overabundant sea urchin (class *Echinoidea*) populations by reducing the prevalence of predatory species such as Atlantic cod (Steneck *et al.*, 2002; Wilmers *et al.*, 2012). Despite the threats these factors pose to global kelp forests, there are few programmes monitoring kelp distribution (Smale *et al.*, 2013; Mora-Soto *et al.*, 2020). This critically impedes conservation efforts (Smale *et al.*, 2013).

Standardised monitoring is required to recognise the decline of kelp communities, particularly within UK sub-littoral zones which contain 50% of North Atlantic seaweed species (Yesson *et al.*, 2015a; Teagle *et al.*, 2017). There are 19,000km^2 of potential kelp habitat around British and Irish coastlines (Yesson *et al.*, 2015b). However, due to the inaccessibility of marine ecosystems, UK kelp distributions are largely unmonitored (Smale *et al.*, 2013; Yesson *et al.*, 2015b). It is especially important that standardised sublittoral monitoring is carried out in southern England, where UK kelp abundance has rapidly declined (Yesson *et al.*, 2015a).

Of the 13 species of kelp found in European waters, three are present along the Sussex coastline, in southern England; tangleweed (*Laminaria hyperborea*), oarweed (*Laminaria digitata*) and sugar kelp (*Saccharina latissima*; Sussex Inshore Fisheries and Conservation Authority, 2020). Until the late 1980s, kelp forests were an abundant habitat in this area, covering approximately 177km^2 (Davies and Nelson, 2019). In the 1970s, an increase in trawling led to a reduction in kelp forest extent and productivity (Davies and Nelson, 2019). The combination of increasing pressure from fishing practices, the 1987 Great Storm, and reductions in water quality has led to a decline of kelp extent by approximately 95% (Sussex Inshore Fisheries and Conservation Authority, 2020). The most recent estimations of remnant kelp patches totalled 6.28km^2 in 2010 (Williams and Davies, 2019). Fishing pressure remains a significant threat to remnant kelp, with six coastal communities having active fishing fleets, including 53 trawling vessels (Williams and Davies, 2019). Therefore, these pressures have resulted in the significant alteration of sublittoral habitats in southern England and the loss of ecosystem functioning (Hiscock *et al.*, 2004).

Restoration of kelp to historic distributions could provide significant benefits (Sussex Inshore Fisheries and Conservation Authority, 2020). Williams and Davies (2019) valued the current ecosystem services of kelp within Sussex as £79,170 per annum. This took into account its yield,

support of commercial fisheries, coastal defence, carbon sequestration and maintenance of water quality (Williams and Davies, 2019). This is significantly lower than the annual ecosystem services value for 1987 kelp forest distributions, valued at £3,630,605. If restored to its current hypothetical maximum, ecosystem services could rise to £3,243,886 (Williams and Davies, 2019). Sussex Inshore Fisheries and Conservation Authority (IFCA) have proposed a bylaw banning trawling within 4km of the Sussex coastline, which was locally approved in 2020 and currently awaits ministerial approval. (Williams and Davies, 2019). This would protect 308km^2 of habitat to facilitate the natural recovery of kelp forests (Williams and Davies, 2019). To monitor kelp abundance and assess the effectiveness of conservation management, remote sensing is often used (Deysher, 1993; Bennion *et al.*, 2019). However, current methodologies and community assessments are based on ad hoc studies, and there is an urgent need for the establishment of a standardised, sublittoral monitoring method for kelp communities (Yesson *et al.*, 2015a; Bennion *et al.*, 2019).

Remote sensing is a rapidly emerging tool for conservation research (Turner *et al.*, 2003; Pettorelli, Safi and Turner, 2014). Since the 1970s, studies on kelp using remote sensing have predominantly used satellites to monitor inaccessible sublittoral communities over large spatial scales (Jensen, Estes and Tinney, 1980; Deysher, 1993; Bennion *et al.*, 2019). Resulting imagery can be used to detect macroalgae and produce species distribution models (SDMs) to aid conservation (Jensen, Estes and Tinney, 1980; Belsher and Mouchot, 1992; Deysher, 1993; Guillaumont, Callens and Dion, 1993). However, due to varying requirements in monitoring kelp under different sublittoral conditions, there is no standardised methodology (Kellaris *et al.*, 2019; Mora-Soto *et al.*, 2020).

1.1 Aims and Objectives

In this thesis, I aim to develop a remote sensing-based monitoring method and produce a distribution estimate for kelp along the Sussex coastline. I then aim to apply this to investigate the extent to which current kelp distributions are impacted by anthropogenic fishing activities. This will be undertaken via several methods of classifying satellite imagery, testing resultant kelp distribution models against ground truthing data, and comparing the area of kelp patches with the spatial distribution of fishing activities. I investigate the hypotheses that: i) satellite imagery can be used to provide a reliable estimate of kelp distribution, and that ii) fishing activities continue to impact kelp along the Sussex coastline.

2 Methodology

2.1 Study area

I conducted this study on approximately 200km of Sussex coastline, covering an area of 10,463km^2. I collected data layers within a study area polygon created in QGIS 3.0.2 (QGIS Development Team, 2020), and cropped layers to a polygon of land above the mean (springs) high water height (Holmes, 2017) using the package 'raster' v3.3-13 (Hijmans, 2020). To give an accurate representation of spatial scale, I reprojected data from the global projection system WGS84 to the local projection system British National Grid, interpolating new values from the original data, using the package 'rgdal' v1.5-15 (Bivand, Keitt and Rowlingson, 2020). Analyses were performed in R v3.6.0 (R Core Team, 2019) using RStudio v1.3.1056 (RStudio Team, 2020).

Figures were created using the package 'ggplot2' v3.3.2 (Wickham, 2016), with north arrows and scale bars added using the packages 'GISTools' v0.7-4 (Brunsdon and Chen, 2014) and 'ggspatial' v1.1.4 (Dunnington, 2020). Data labels were added using the 'ggrepel' v0.8.2 (Slowikowski, 2020) package, and accessible palettes were used through the package 'RColorBrewer' v1.1-2 (Neuwirth, 2014).

2.2 Ground truthing data

I collated ground truthing points from towed video collected by Sussex IFCA and Zoological Society of London (ZSL) on 21st April 2013, cleaning and manipulating dataframes using the packages 'tidyr' v1.1.0 (Wickham and Henry, 2020), 'dplyr' v1.0.1 (Wickham *et al.*, 2020), 'data.table' v1.13.0 (Dowle and Srinivasan, 2020), and 'varhandle' v2.0.5 (Mahmoudian, 2020). A sledge mounted camera was towed along the seabed at a constant speed. This was attached to a research vessel by a cable approximately 10m long. Surveying occurred at 16 stations (transects) off Selsey. The research vessel recorded depth, time and coordinates at the start and end of each transect. Coordinates were corrected to estimate the position of the towed camera (Figure 1). This lag in position (1) was calculated, based on Pythagoras' theorem, and using known depth (Z) and cable length (C) values, assuming the cable to be virtually straight, as:

$$Lag^2 = Z^2 + C^2 \quad (1)$$

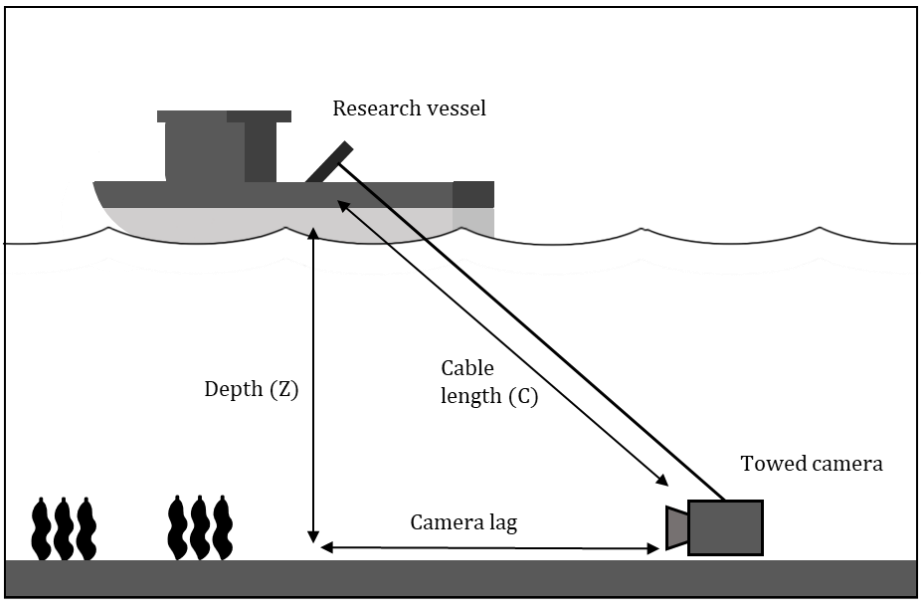

Figure 1: Diagram illustrating towed camera surveys carried out to detect kelp (*Laminaria* spp.), with the camera position calculated using known values of cable length and depth.

Still images were extracted from the footage at approximately 20s intervals, selected when the seabed was clearly visible. For each image, the time and species present were noted. For use in figures, percentage cover was noted and translated into abundance using the SACFOR abundance classification scale for sublittoral flora (Hiscock, 1996). The time elapsed per image was multiplied by speed to calculate the distance along the transect, using the package 'chron' v2.3-55 (James and Hornik, 2020). This was combined with start coordinates of the boat, camera lag and bearing to provide coordinates for each image using the package 'geosphere' v1.5-10 (Hijmans, 2019) to account for the earth's curvature. I used this method to analyse data from three stations and was provided with pre-analysed data for 13 stations by ZSL. I plotted these coordinates as vector data (spatial coordinates) using the packages 'sp' v1.4-2 (Pebesma and Bivand, 2005) and 'sf' 0.9-5 (Pebesma, 2018), and assigned a binary value, kelp present or absent, depending on whether the image contained kelp.

I collated observations of *Laminaria* spp. based on records taken by divers (Seasearch, 2019), from the biodiversity recording website, National Biodiversity Network Atlas (NBN; 2020). While the spatial accuracy of these observations was too low for analysis (>10m), they were used to illustrate possible kelp distribution. I removed observations taken prior to the year 2000, that were considered unlikely to represent current distributions.

2.3 Remote sensing data

Imagery, collected by the Sentinel satellite constellation, was collated by myself from the Copernicus Open Access Hub (European Space Agency, 2020a). At a 10x10m resolution, four spectral bands

were available (Red, Green, Blue and Near Infra-Red), with six additional bands (four visible and near-infrared, and two short-wave infrared bands) at 20x20m resolution (European Space Agency, 2020a, Supplementary Information 1). I selected Sentinel Level 2a imagery which provided bottom-of-atmosphere reflectance values with atmospheric water vapour correction and orthorectification (correcting for perspective) carried out (European Space Agency, 2015). I extracted, and combined by date, image tiles unobscured by dense cloud (<30% coverage). I calculated mean windspeed and wave height, factors which increase turbidity and suspended sediment in the water column, using records from the Chimet weather buoy, situated at the mouth of Chichester Harbour (Chimet Support Group, 2020). These values were calculated for two days prior to image collection. I took tide height at the time of data collection for Selsey from Tides4Fishing (Tides4Fishing, 2020). Reflectance values extracted from satellite images with high turbidity or suspended sediment in the water column were likely to be non-representative of the seabed. I selected multiple images where conditions minimised water depth, turbidity, and suspended sediment, and plotted them as spatial raster data (pixel-based imagery) using the 'raster' package.

From Edina Digimaps (OceanWise, 2016), I sourced a 30x30m resolution Digital Elevation Model raster showing bathymetry (seabed depth) which was created by OceanWise, based on combined multibeam acoustic and LIDAR data. I altered bathymetry using bilinear interpolation to match the satellite imagery resolution, creating more pixels with the same values, using the package 'gdalUtils' v2.0.3.2 (Greenberg and Mattiuzzi, 2020).

I sourced vector data identifying seabed sediment classes from Edina Digimaps, created by British Geological Survey based on sediment samples (British Geological Survey, 2011). Raster data of 25x25m resolution quantifying fishing activity over 1,706.74km^2 of the study area, was provided by ZSL. This data calculated fishing activity as the annual average number of fishing vessels observed, based on vessel GPS tracking data collected by Global Fishing Watch (Global Fishing Watch, 2020).

2.4 Image classification

I ran three pixel-based classification methods commonly used to study kelp: an index classification (Hu, 2009; Garcia and Sitjar, 2020; Mora-Soto *et al.*, 2020), alongside two machine learning algorithms; a supervised (Casal, Sánchez-Carnero, *et al.*, 2011; Brodie *et al.*, 2018; Kellaris *et al.*, 2019) and unsupervised classification (Van der Wal *et al.*, 2014; Yesson, Ash and Brodie, 2015). For index-based classification, I used the Kelp Difference index (KD), designed to identify the spectral signature of kelp (Mora-Soto *et al.*, 2020). KD (2) was calculated as the difference in reflectance values between infra-red (R_{B6}), and red (R_{B4}) satellite image bands:

$$KD = R_{B6} - R_{B4} \quad (2)$$

Unsupervised classification was conducted using machine learning algorithms which classify image pixels based on a specified number of clusters. K-means clustering partitions data into a specified

number of clusters by maximising intra-class similarity and minimising inter-class similarity (MacQueen, 1967). This algorithm randomly selected observations as cluster centroids and assigned observations to clusters by minimising the Euclidean distance between the observation and the centroid. New cluster centroids (means) were then calculated. Clustering Large Applications (CLARA) is a similar method designed to deal with large datasets (>1,000 observations; Kaufman and Rousseeuw, 1990). This algorithm randomly subsampled the data, creating a specified number of clusters. One observation per cluster was randomly selected as a medoid, an observation within the dataset with minimal dissimilarity between all observations within the cluster. The entire dataset was then assigned to medoids. Both algorithms iterated until cluster assignments converged. I repeated K-means and CLARA clustering, specifying 2-8 clusters based on Van der Wal *et al.* (2014), using the package 'cluster' v2.1.0 (Maechler *et al.*, 2019). I selected the clustering algorithm and number of clusters which maximised the highest average similarity of observations to their clusters (silhouette index), using the packages 'clusterCrit' v1.2.8 (Desgraupes, 2018) and 'knitr' v1.29 (Xie, 2020). I assigned clusters as kelp present/absent, depending on which cluster included the most ground truthing observations of kelp.

Supervised classification was conducted using a Support Vector Machine (SVM) learning algorithm which produces a predictive model trained on ground truthing data. To train the model, I extracted the median cell values of each satellite image within a 10m radius (known as a "buffer") of each ground truthing point containing kelp, using the 'raster' package. Cells overlapping the buffer edges were included in the median. I then divided ground truthing points at random, with 25% as a training dataset, and 75% for model validation, based on Brodie *et al*. (2018). I then ran an SVM to find a hyperplane which best differentiated classes within the training dataset, using the package 'e1071' v1.7-3 (Meyer *et al.*, 2019). The hyperplane was determined based on gamma (γ) and cost (C) values. γ determines the influence of individual observations on fitting the hyperplane, which if too large may excessively delineate data and lead to overfitting. C determines the cost of misclassification by specifying the size of the hyperplane margin, within which points may be misclassified. I selected the optimal gamma and cost parameters by testing combinations of a range of values (gamma: 2^{-13}-2^{10} cost: 2^{-5}-2^{10}) to produce predictions with the highest percentage agreement with training data. I then ran the SVM using the optimal parameters, which predicted classes across the entire satellite image.

I ran all three classification methods on each satellite image. To test the accuracy of models against ground truthing points, I extracted the median cell values of each model within a 10m buffer of each point. A 10m buffer was chosen to match model resolutions. For supervised classification models, I used 75% of the ground truthing data (see above). I then assigned these values a binary predicted category, kelp present or absent. I created a confusion matrix for each model run on each satellite image, comparing expected categories from ground truthing data to categories predicted by the model. These matrices, using the number of observations (N) and categories (k), gave the number

of times the final model (i) correctly predicted category (n_{ki}). I then calculated (3) the probability of agreement (P_o), and (4) probability of random agreement (P_e), to produce (5) a Cohen's Kappa value (Cohen, 1960) to test whether satellite imagery can provide a reliable estimate of kelp distribution:

$$P_o = \frac{n_{ki}}{N} \quad (3)$$

$$P_e = \frac{1}{N^2} \sum_k n_{k1} n_{k2} \quad (4)$$

$$Kappa = \frac{P_o - P_e}{1 - P_e} \quad (5)$$

Kappa values of 1 suggested a perfect agreement between a model and ground truthing data. I then selected the model and satellite image with the highest Kappa value to predict kelp distribution.

2.5 Water attenuation correction

Light passing through a water column is attenuated (absorbed and scattered) due to suspended material and the refractive properties of water (Kirk, 1994). Therefore, it may be important to correct this effect in data in order to produce accurate classifications (Kirk, 1994). Lyzenga's equation (Lyzenga, 1978, 1981) is the most commonly used method to correct for light attenuation in the water column and increase the accuracy of seabed classification (Zoffoli, Frouin and Kampel, 2014). This was adapted by Sagawa *et al.* (2010) to study coastal ecosystems, accounting for water with low transparency by including depth:

$$X_i = \frac{(L_i - L_{si})}{\exp(-K_i g Z)} \quad (6)$$

The corrected values of seabed reflectance (X_i) were calculated for each satellite image spectral band (i) using reflectance (L_i), deep water radiance (L_{si}), the rate of light attenuation in the water column (K_i, attenuation coefficient, m^{-1}), the path length of light passing through the water column (g) and water depth (Z). I extracted depth data (Z) from the bathymetry raster and added tide height at the time the satellite image was collected using the 'raster' package. I assumed that Z was equivalent to g and therefore, to produce negative depth values, took g as -1. I calculated attenuation coefficients (K_i) by assuming that variations in reflectance values over bare sand were due to attenuation over varying water depths. I identified bare sand as points in QGIS, where the seabed was classed as sand by sediment vector data and where sand was visually identifiable in satellite imagery. To find the rate of light attenuation, I ran a linear model, taking reflectance value as the response variable, and depth as the explanatory variable, for each spectral band of the satellite imagery. To give an indication of correction accuracy, I compared the expected relative attenuation rates for the spectral bands to the model slopes. I calculated deep-water radiance (L_{si}) by taking the mean reflectance values for deep-water areas within the lowest 10th percentile of depth values,

based on Sagawa *et al.* (2010), using the packages 'raster' and 'maptools' v1.0-1 (Bivand and Lewin-Koh, 2020). To test whether water attenuation correction was necessary, I used these values to calculate (6) for the satellite image which had produced models with the highest Kappa values. I then repeated image classification on the corrected image. If corrected imagery produced higher Kappa values than corresponding uncorrected imagery, then the attenuation correction increased the accuracy of predicted kelp distribution and was retained.

2.6 Data analyses

To check whether the model erroneously predicted sediment class, I transformed sediment vector data into a raster using the package 'fasterize' v1.0.3 (Ross, 2020), and compared class predicted by the final model using a Kruskal-Wallis test. Effect size was quantified using an epsilon-squared test (ε2; Kelley, 1935) and a *post hoc* Mann-Whitney U was used to test the pairwise differences between sediment classes, using the package 'rcompanion' v2.3.25 (Mangiafico, 2020). To check the consistency of models, and therefore the likelihood that each model predicted kelp rather than random "noise", I calculated a pairwise Schoener's D metric (7). Schoener's D gives the niche overlap between two spatial distribution models (Z_{1ij} and Z_{2ij}), accounting for spatial autocorrelation, with values of 1 indicating identical overlap (Schoener, 1970):

$$D = 1\frac{1}{2}\left(\sum_{ij}\left|Z_{1ij} - Z_{2ij}\right|\right) \quad (7)$$

This was conducted on all models produced with the final (most accurate) classification method, using the package 'fuzzySim' v3.0 (Barbosa, 2015). I aggregated the final model and fishing activity rasters into 50x50m resolution grids, with each new cell taking the sum and mean of the corresponding original cell values, respectively, using the 'gdalUtils' and 'raster' packages. I then cropped the final model to match the extent of fishing data, and multiplied cell values by model resolution (10*10) to give kelp cover in m^2 for each cell.

To test if the area of kelp forest was associated with fishing activity, I ran a generalised linear model using the package 'lme4' v1.1-23 (Bates *et al.*, 2015). Poisson distributed kelp area (m^2) was taken as the response variable, and fishing activity as the continuous explanatory variable. Plotting data showed that kelp area was zero inflated, and therefore a Poisson, and a zero inflated Poisson model were run using the 'pscl' v1.5.5 (Zeileis, Kleiber and Jackman, 2008) and 'performance' v0.4.8 (Lüdecke *et al.*, 2020) packages. To check that the model assumption of normally distributed residuals was not violated, I inspected model diagnostic plots. The likelihood ratio test and a comparison of model AIC values were used to select the model which best fitted the data using the 'lmtest' v0.9-37 package (Zeileis and Hothorn, 2002). I reported results as statistically significant if $p \leq 0.05$ and plotted model coefficients using the package 'sjPlot' v2.8.4 (Lüdecke, 2020).

3 Results

3.1 Ground truthing data

Ground truthing from towed camera surveys included kelp presence observations, (n=74) averaging 6.17 observations per transect (SD: 5.57, range: 1-17), and kelp absence observations (n=113). Additionally, I collated 154 observations of kelp from NBN (Figure 2).

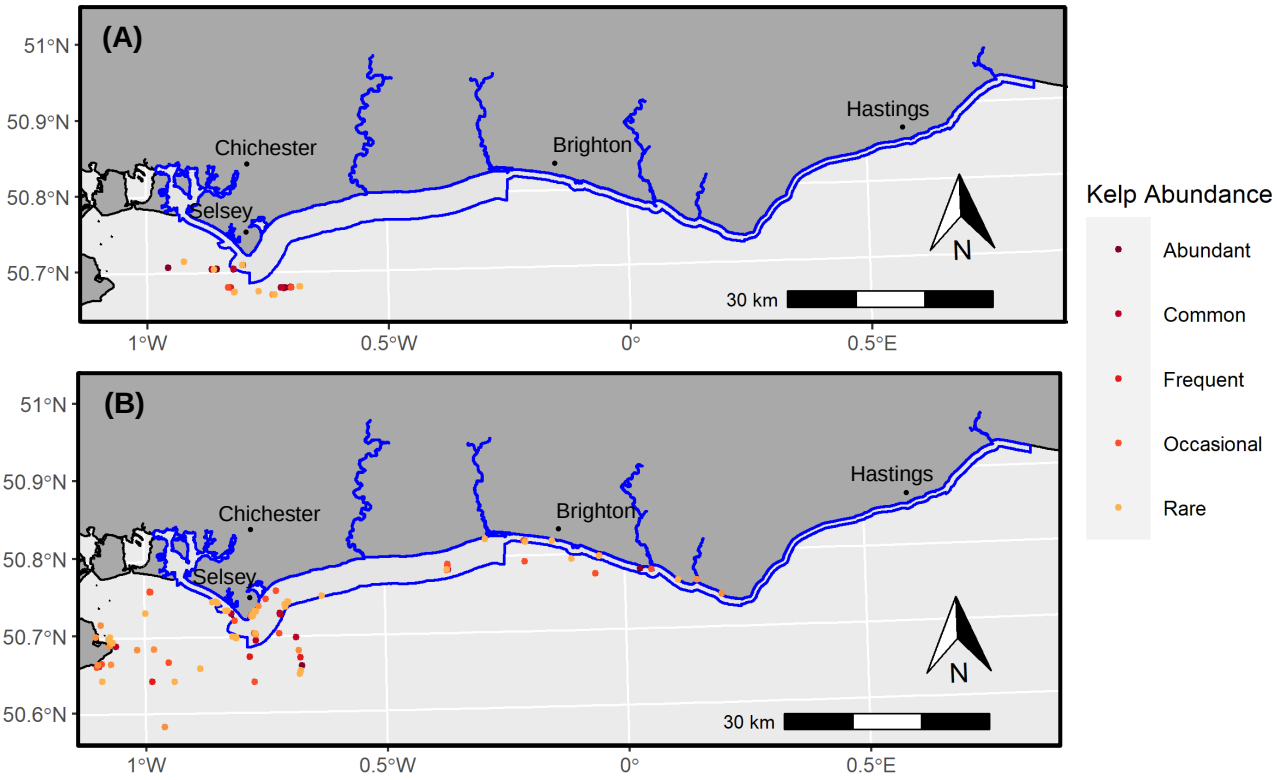

Figure 2: Maps of kelp (Laminaria spp.) presence along the Sussex coast, coloured by abundance. Data were based on (A) towed camera surveys carried out by Zoological Society of London and (B) citizen science data from divers collated from National Biodiversity Network (2020). The blue line indicates the area where trawling will be banned to protect kelp.

3.2 Remote sensing data

Of the satellite images collated (N=7), four were collected during suitable conditions and used for classification (Supplementary Information 2). These images were acquired on 20.07.2020, 21.04.2020, 26.02.2019, and 22.04.2018.

3.3 Image classification

Unsupervised classifications, using two clusters (Supplementary Information 3), and the Kelp Difference index both produced Kappa values of zero, indicating no agreement with ground truthing data (Table 1, Figure 3; Cohen, 1960). Supervised classifications produced the highest Kappa values, with the image collected on 26.02.19 producing a Kappa value of 0.46, indicating a "moderate" agreement with ground truthing data (Table 1; Cohen, 1960). Therefore, this species distribution model was considered the most accurate predictor of kelp and was used for further analysis (Figure 3).

Table 1: Accuracy and diagnostic values for classification models performed on satellite images collected on a range of dates. Kappa values indicate the agreement between models and ground truthing data. Diag values indicate the percentage of observations used for calculation. Rand and crand values indicate the similarity between clusters, with crand values corrected for chance agreement

		Satellite image acquisition date			
Classification		*20.07.20*	*21.04.20*	*26.02.19*	*22.04.18*
Kelp Difference Index	diag	0.41	0.41	0.41	0.41
	Kappa	0.00	0.00	0.00	0.00
	rand	0.51	0.51	0.51	0.51
	crand	0.00	0.00	0.00	0.00
Unsupervised	diag	0.40	0.40	0.41	0.4
	Kappa	0.00	0.00	0.00	0.00
	rand	0.52	0.52	0.51	0.52
	crand	0.00	0.00	0.00	0.00
	Selected algorithm	CLARA	K-Means	K-Means	K-Means
	N. clusters	2.00	2.00	2.00	2.00
Supervised	diag	0.68	0.71	0.75	0.73
	Kappa	0.28	0.37	0.46*	0.43
	rand	0.56	0.59	0.62	0.61
	crand	0.12	0.17	0.24	0.21
	Gamma value	1024.00	0.03	0.50	2.00
	Cost value	2.00	1024.00	1.00	1.00

*Final selected model

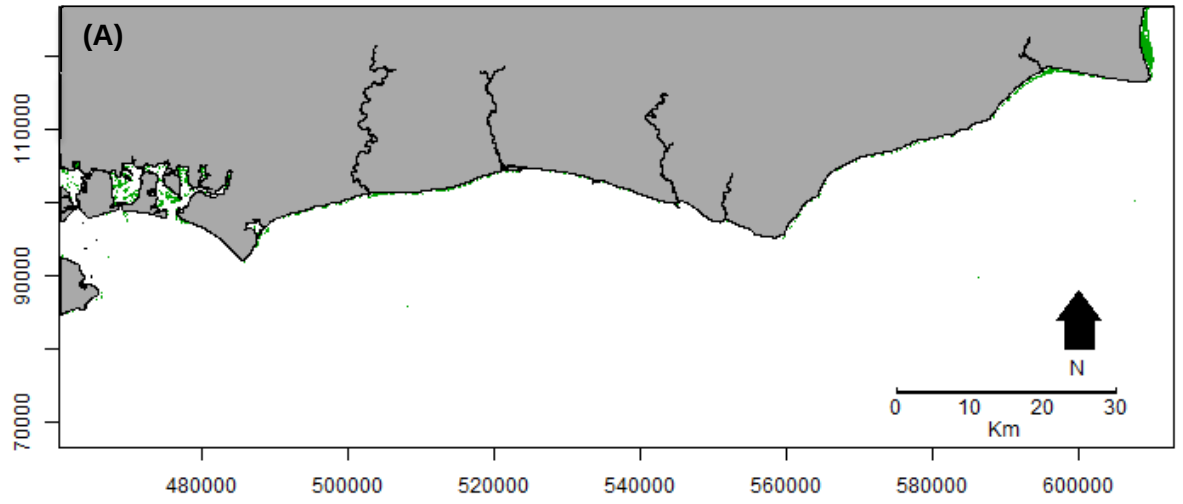

344

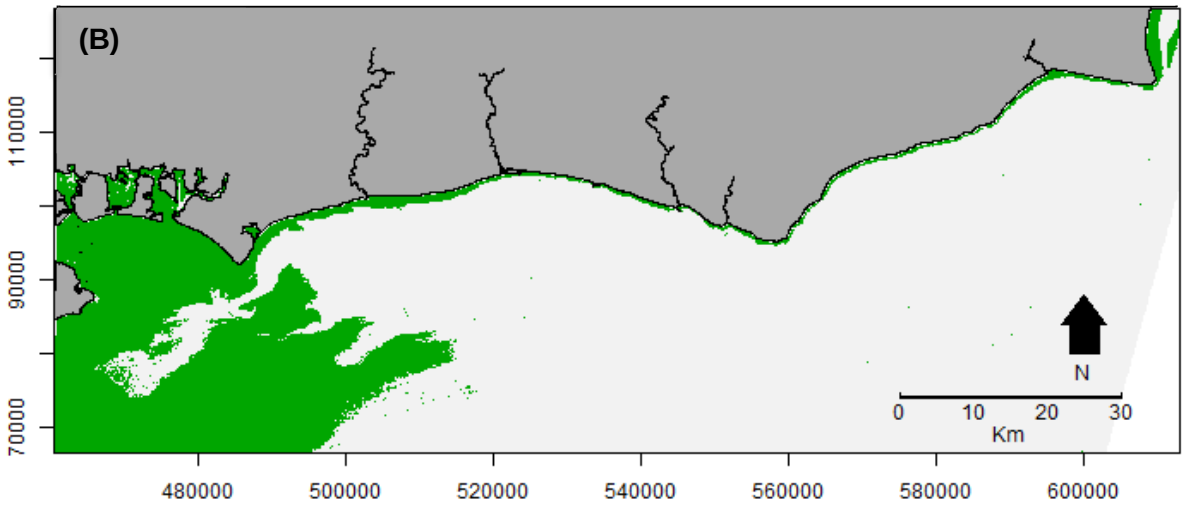

345

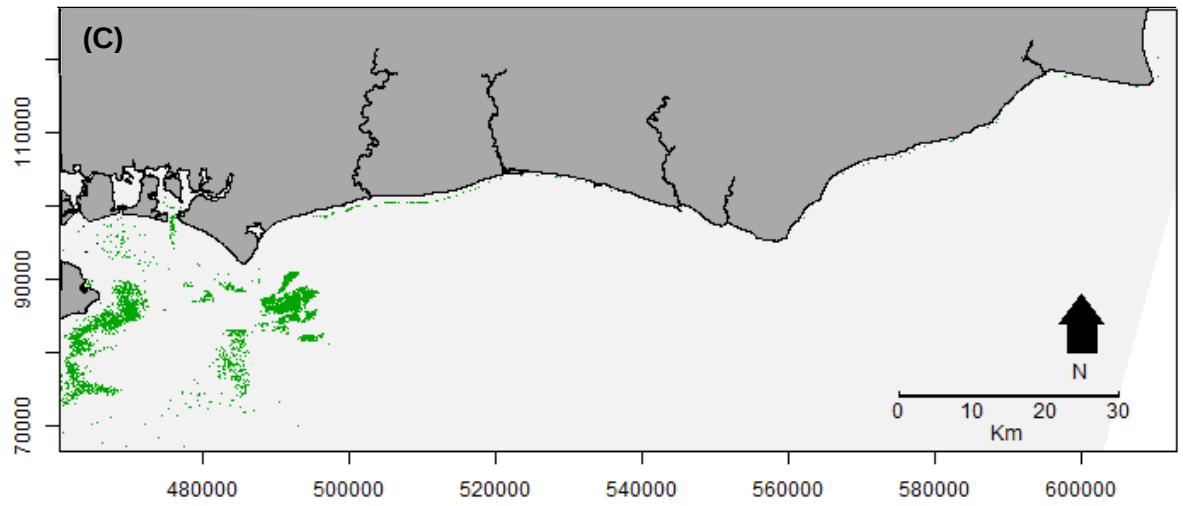

346

Figure 3: Species distribution models for kelp (*Laminaria* spp.) along the Sussex coast, with green cells indicating predicted kelp presence. These models were based on satellite imagery collected on 26.02.19, produced using (A) the Kelp Difference Index, (B) an unsupervised classification, and (C) a supervised classification.

3.4 Water attenuation correction

I ran the water attenuation correction on the image collected on 26.02.19, which produced the most accurate model during classification. I identified 20 points on bare sand (Supplementary Information 4). Linear models taking logged satellite band values as the response variable, and depth as the explanatory variable, showed the rate of light attenuation in the water column for bare sand points (Figure 4, Supplementary Information 5). These models met the expectation that near infra-red light is attenuated most rapidly.

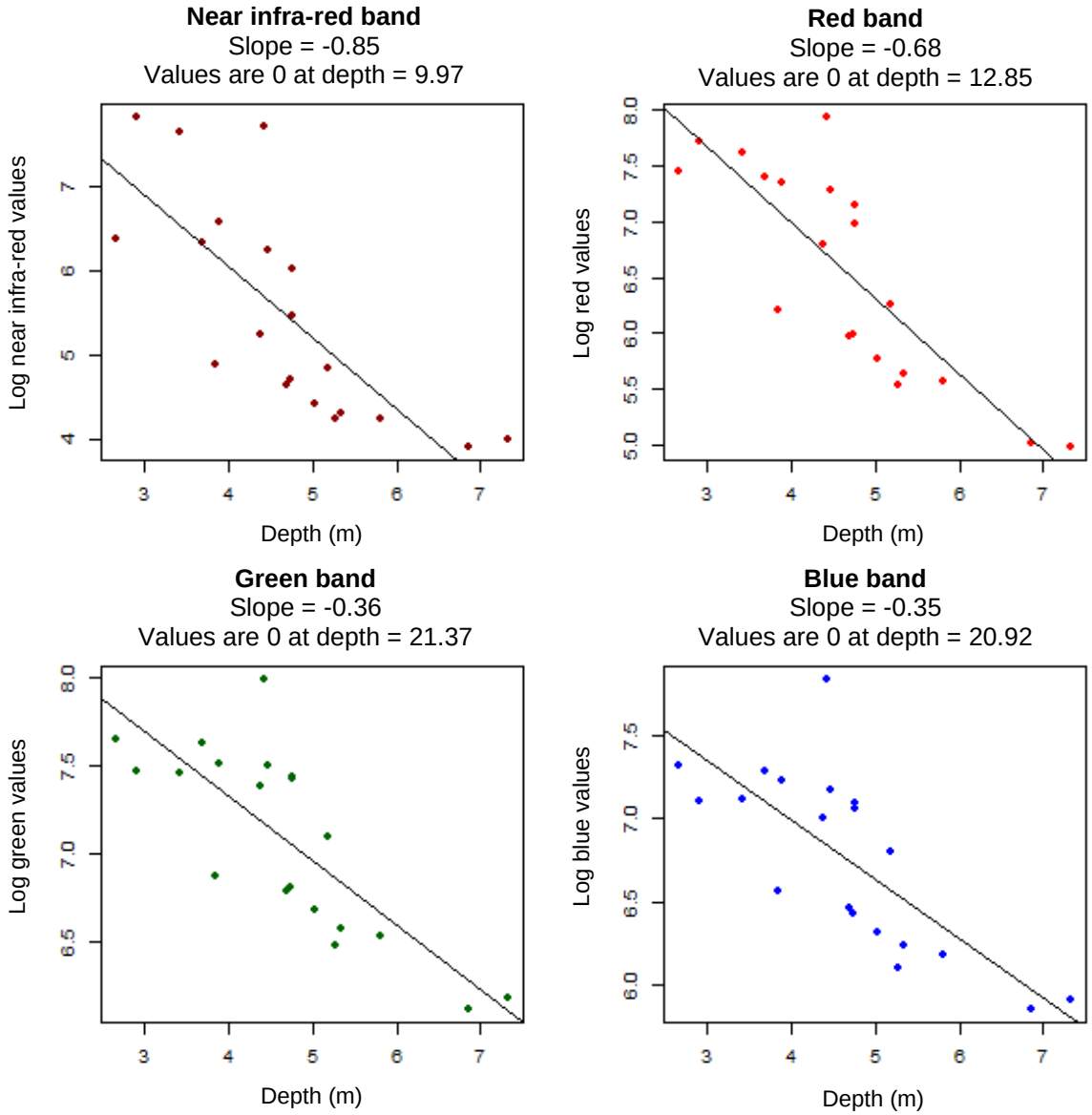

Figure 4: Linear regressions showing the rate of light attenuation through the water column (attenuation coefficients) for bare sand at varying depths. Logged values for each light band are taken as the response variables, and depth as the explanatory variable.

The correction produced a new image, with deep-water values becoming zeros (Supplementary Information 6). This therefore appeared to visually homogenise large sections of the corrected image

(Figure 5). Image classification run on the corrected satellite image produced Kappa values of zero for each method. Therefore, the correction did not improve classification accuracy and was discarded for further analysis.

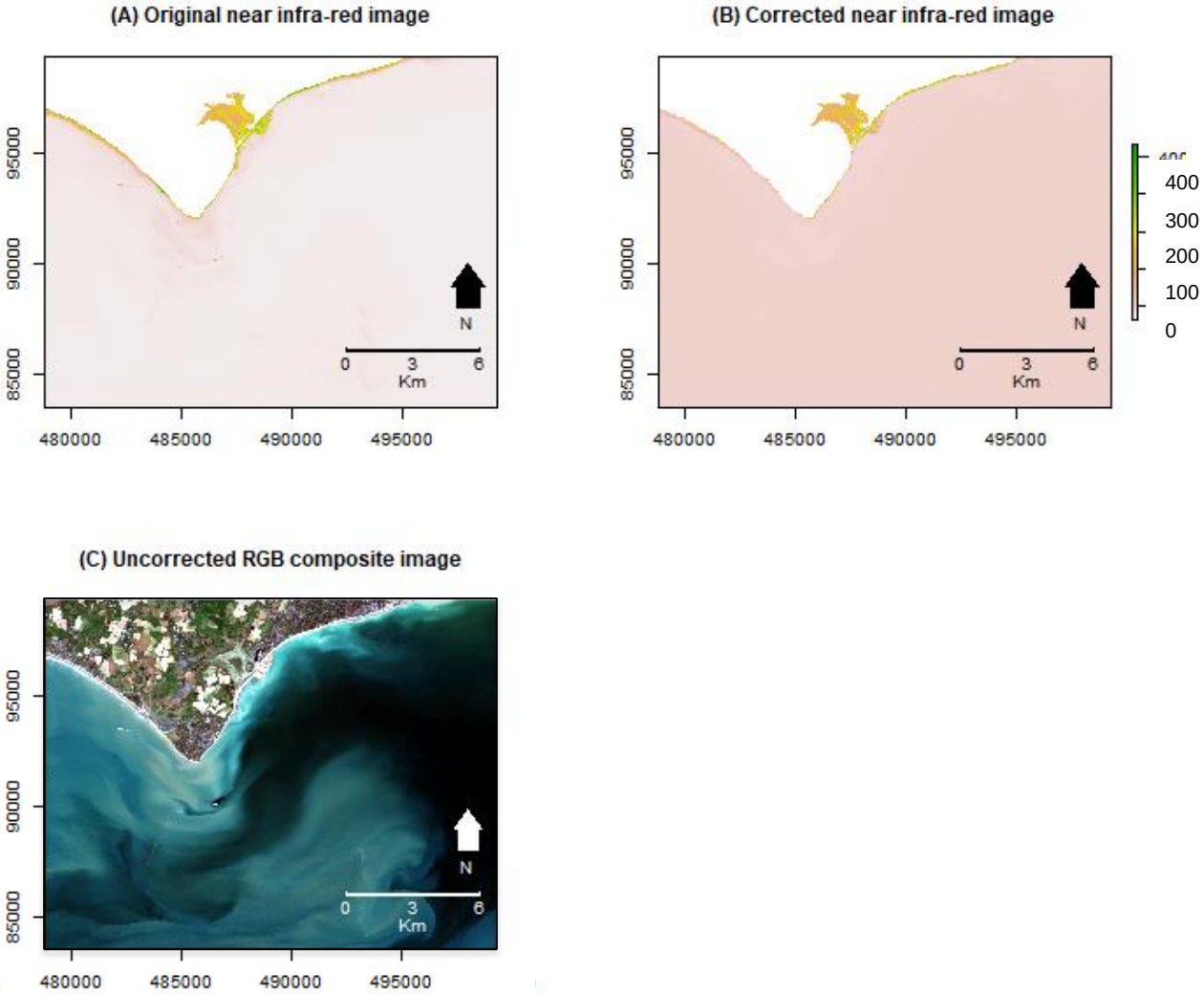

Figure 5: Satellite imagery for the sea off Selsey within the study area, showing (A) near infra-red reflectance values compared to (B) corresponding values corrected for light attenuation within the water column, and (C) a composite (red, green, blue) true colour image based on original reflectance values.

3.5 Data analyses

The final model predicted 100.13km^2 of kelp present within the study area (Figure 6). There was a difference in the final model prediction between sediment classes (Kruskal-Wallis, N=505,543,748, chi-squared=575,643, df=12, p<0.001), however the effect size was small (ε^2=0.01). Kelp occurred most frequently in sandy gravelly mud and muddy sandy gravel (p<0.001; Supplementary Information 7). Furthermore, supervised classification models had low consistency for each pairwise comparison between different dates (Table 2).

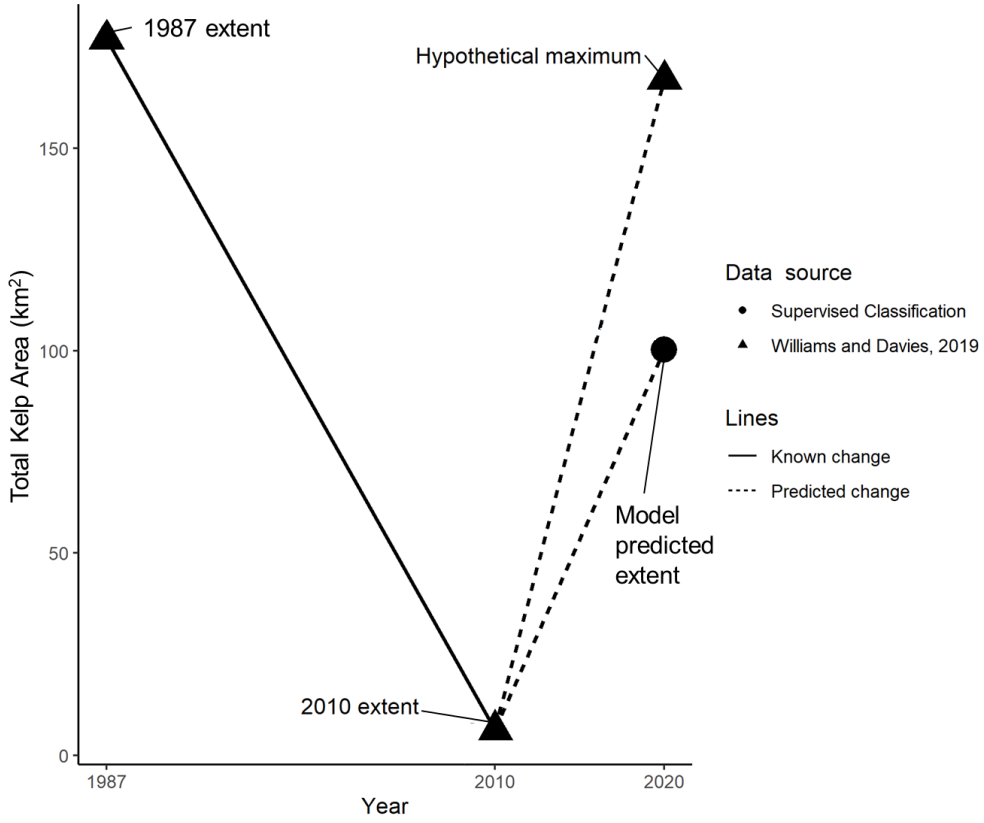

Figure 6: Graph showing the change in kelp (*Laminaria* spp.) area present along the Sussex coastline, compared to the area predicted by a supervised classification model.

Table 2: Correlation matrix for supervised classification models for satellite imagery, produced using the Schoener's D metric for spatial niche overlap, with values of 1 indicating identical overlap (Schoener, 1970).

Satellite imagery acquisition date	22.04.18	26.02.19	21.04.20	20.07.20
22.04.18	–	0.01	0.02	0.03
26.02.19	0.01	–	0.04	0.01
21.04.20	0.02	0.04	–	0.09
20.07.20	0.03	0.01	0.09	–

For the linear model using observations taken per 50*50m area (N=591,654), the average area of kelp was 113.24m^2 (SD: 454.95, range: 0.00-2500.00) and average fishing activity was 3.90 (SD: 6.50, range: 0.00-72.71, Figure 7). Goodness of fit was assessed, and a zero-inflated Poisson model selected (likelihood ratio test, chi^2 = 2.65x10^8, df = 2, p=<0.001). I found a positive, statistically significant association between predicted kelp area and observed fishing activity (Table 3). An increase in 1 vessel/year resulted in a 92% increase in kelp area. An adjusted R^2 of 1.00 indicated the model fit the data well.

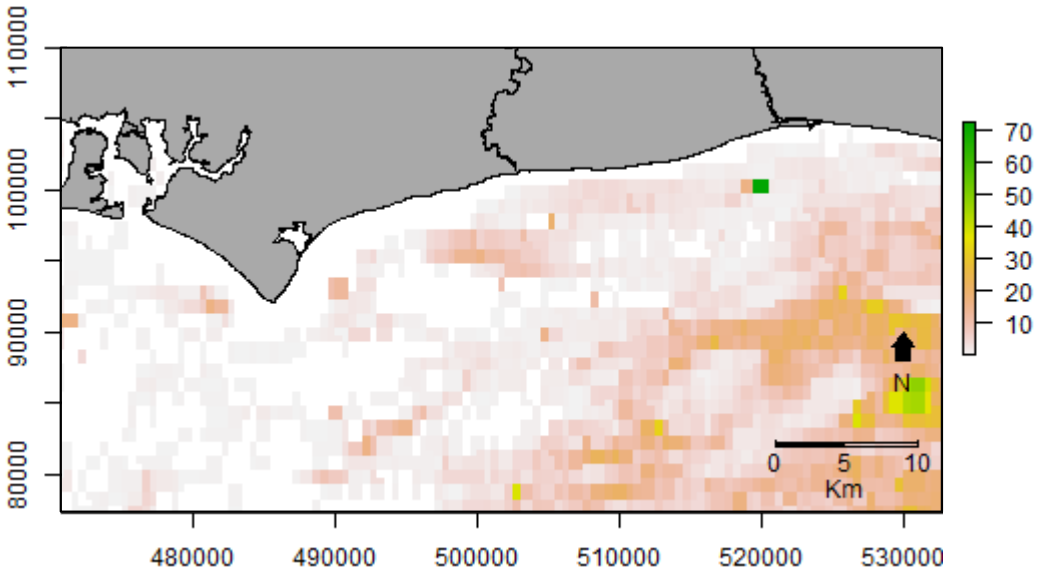

Figure 7: Raster data showing fishing activity. This was calculated as the average annual number of fishing vessels observed per 25x25m cell, based on vessel GPS tracking (Global Fishing Watch, 2020).

377

Table 3: Outputs of a linear regression (zero-inflated Poisson model) showing how area of kelp (*Laminaria* spp.) forest is associated with fishing activity (average vessels/year).

	Kelp area (m^2)		
Predictors	*Incidence Rate Ratios*	*CI*	*p*
(Intercept)	4.97	4.92 – 5.03	**<0.001**
Fishing activity	1.92	1.90 – 1.94	**<0.001**
Observations	591,654		
R^2 / R^2 adjusted	1.00 / 1.00		

378

379

380

381

382

383

384

4 Discussion

In this thesis, I evaluated remote sensing-based methods commonly used to monitor kelp distribution and identify supervised classification as the most appropriate for studying kelp in Sussex. I produced a species distribution model for kelp and found that kelp distribution is related to anthropogenic fishing activity along the Sussex coastline.

The final species distribution model predicted kelp with an accuracy comparable to Kappa values reported by other studies (Van der Wal *et al.*, 2014; Brodie *et al.*, 2018; Mora-Soto *et al.*, 2020). However, while Kappa values are the most common statistic used to report classification accuracy, several studies suggest that their categorisation is lenient, allowing inaccurate models to be treated as accurate (Bruckner and Yoder, 2006; McHugh, 2012). Following the suggested categorisation of Kappa values by McHugh (2012), the agreement between ground truthing data and my final SDM would instead be classed as “weak”, suggesting that my model should be treated with caution. My final SDM predicts kelp in areas of historic kelp distribution (Williams and Davies, 2019) and follows a similar distribution to citizen science data (Figure 2). However, my model suggests that kelp forest area has recovered by 1,594% since 2010. While this is lower than the hypothetical maximum distribution of kelp, the recovery predicted by my model is unlikely as there has been little conservation action or alteration to fishing pressure (Williams and Davies, 2019).

My results showed that fishing activity was significantly positively associated with kelp presence. This suggests that fishing activity is directed towards areas of remnant kelp forest, and therefore fishing continues to impact kelp along the Sussex coast. Further research is required to determine relationship directionality, which may also be due to fishing activity promoting kelp development. However, this is highly unlikely as studies have shown kelp forests take several years to recover from damage caused by trawling (Christie, Fredriksen and Rinde, 1998; Steen *et al.*, 2016). It is also possible that my model erroneously predicts features other than kelp, such as different algal species or the elevated roughness of trawled seabed (Smith *et al.*, 2003; Brodie *et al.*, 2018). If model variables are both indicators of fishing activity, this would explain the biologically improbable high R^2 value (Table 3). However, any conclusions drawn from the correlation between fishing and kelp distribution are limited by the low accuracy of my final model.

4.1 Limitations

The low accuracy of my model may be due to multiple factors such as patches of kelp smaller than imagery pixels, which may result in the misclassification of features other than kelp (Brodie *et al.*, 2018). While the model predictions differed between sediment classes, this may be due to the high sample size resulting in a false positive result, and the effect size was small. Similarly, high turbidity may reduce the visibility of the seabed through the water column (Kutser, Vahtmäe and Martin, 2006). The attenuation correction found that light was attenuated at shallower depths than many

kelp patches identified by ground truthing. Near infra-red and red bands are important in detecting kelp and other vegetation (Hu, 2009; Mora-Soto *et al.*, 2020). However, these bands were affected by high rates of light attenuation, suggesting that deep areas had "true" reflectance values of zero. Models may therefore be classifying spectral noise, values not representative of the seabed, supported by the low consistency between models (Sagawa *et al.*, 2010). This would explain the failure of the Kelp Difference Index, unsupervised classification, and water attenuation correction, to produce Kappa values greater than zero. Due to low model accuracy, this study cannot accept the hypotheses that satellite imagery can be used to provide a reliable estimate of kelp distribution and is unable to determine whether fishing activities continue to impact kelp along the Sussex coastline.

My model's accuracy could be improved by multiple methods. More ground truthing data, collected recently and with a wider distribution across the study area, may provide a training dataset more representative of the spectral signature of kelp in Sussex and improve supervised classification (Abburu and Golla, 2015). Similarly, the Kelp Difference Index was designed to identify the spectral signature of giant kelp (*Macrocystis pyrifera*; Mora-Soto *et al.*, 2020). An index adjusted to identify the spectral signature of kelp species present in Sussex (tangleweed, oarweed and sugar kelp) may increase the accuracy of index-based classification (Hu, 2009). Unsupervised classification is subject to human error during the manual assignment of habitat classes to predicted clusters (Abburu and Golla, 2015), however there was little ambiguity in this study. While each classification may be adapted to improve accuracy, the major limitation to this study was spectral noise within satellite imagery. This study attempted to identify kelp in smaller patches and within deeper water than many concurrent studies (Casal, Sánchez-Carnero, *et al.*, 2011; Mora-Soto *et al.*, 2020). Under such conditions, the lack of accurate seabed reflectance values, along with insufficient resolutions, may have prevented accurate classification (Sagawa *et al.*, 2010; Zoffoli, Frouin and Kampel, 2014). Higher resolution data, collected under suitable conditions to reduce water column turbidity, may ensure the classification of accurate seabed reflectance values and improve model accuracy (Brodie *et al.*, 2018; Bennion *et al.*, 2019).

4.2 Implications and future research

The species distribution model produced by this study does not have sufficient accuracy to inform Sussex IFCA's monitoring programme. At most, this model could be used to inform stratified diving or towed camera surveys to confirm the presence of kelp. My results support Bennion *et al*. (2019), suggesting that traditional, direct observation surveys remain the "gold standard" of monitoring macroalgae due to limited confidence in remote sensing derived predictions. While the lack of standardisation for imagery classification to identify kelp has been criticised by several studies (Bennion *et al.*, 2019; Kellaris *et al.*, 2019; Mora-Soto *et al.*, 2020), the methods used in this study have been previously used to successfully identify kelp distributions in other areas (Yesson, Ash and Brodie, 2015; Brodie *et al.*, 2018; Kellaris *et al.*, 2019; Mora-Soto *et al.*, 2020). I suggest that the

quality of widely available remote sensing data remains the major limitation of remote sensing to produce SDMs for sublittoral kelp. Satellite images for subtidal remote sensing should be selected to account for many confounding factors, including cloud cover, tide height, and sea state (Kutser, Vahtmäe and Martin, 2006; Casal, Sánchez-Carnero, *et al.*, 2011). However, satellite imagery is not targeted at coastal areas, often resulting in suboptimal images with high turbidity and light attenuation (Yesson, Ash and Brodie, 2015; Bennion *et al.*, 2019). This limitation highlights the need for remote sensing methods with high spatial resolutions, targeted to meet the study-specific requirements of monitoring kelp forests.

Remote sensing platforms which offer alternatives to satellites could increase the application of remote sensing. Satellite imagery provides repeated, global coverage with high spectral resolutions (Hu, 2009; Casal, Kutser, *et al.*, 2011; Yesson, Ash and Brodie, 2015; Mora-Soto *et al.*, 2020). However, while continually improving, the spatial resolution of widely available satellite imagery may be insufficient for the detection of small kelp forest patches. While macroalgae SDMs have been produced using satellite imagery with low spatial resolutions (>300m; Kutser, Vahtmäe and Martin, 2006; Hu, 2009), it is not possible to detect patches <10 hectares at resolutions <20m (Deysher, 1993; Kellaris *et al.*, 2019). Planes and drones offer cost effective methods to map kelp distribution at higher resolutions than widely available satellite imagery (<100cm; Deysher, 1993; Volent, Johnsen and Sigernes, 2007; Brodie *et al.*, 2018; Kellaris *et al.*, 2019). Furthermore, unlike satellite orbits, plane and drone surveys may be timed to coincide with optimal tidal and weather conditions, improving classification accuracy (Yesson, Ash and Brodie, 2015; Bennion *et al.*, 2019).

Conservation of global kelp forests is reliant on understanding their distributions to inform conservation efforts. Whilst previous studies have successfully used similar methodologies to map kelp forest distributions, their application is not universal. Discrepancies in the quality of widely available remote sensing data restricts the use of remote sensing to predict kelp forests. Future studies should use the methodology established by this thesis for high resolution monitoring of kelp in Sussex, when such data becomes available. Whilst unable to produce an accurate species distribution model and examine the factors influencing kelp distribution, this thesis highlights the need for higher quality remote sensing imagery in the monitoring of declining kelp forests.

Data and Code Availability

Should the reader wish to view the data used for this study, or reproduce the described analysis, full datasets and R code scripts are available at the following Imperial College London Box link: https://imperialcollegelondon.box.com/s/tz9cj479x2acyjz0rur4gzjpbkhb0b1u

References

Abburu, S. and Golla, S. B. (2015) 'Satellite Image Classification Methods and Techniques: A Review', *International Journal of Computer Applications*, 119(8), pp. 975–8887.

Barbosa, A. M. (2015) 'fuzzySim: applying fuzzy logic to binary similarity indices in ecology', *Methods in Ecology and Evolution*, 6(7), pp. 853–858. Available at: https://besjournals.onlinelibrary.wiley.com/doi/full/10.1111/2041-210X.12372.

Bates, D. *et al.* (2015) 'Fitting Linear Mixed-Effects Models Using lme4', *Journal of Statistical Software*, 67(1), pp. 1–48. doi: doi:10.18637/jss.v067.i01.

Belsher, T. and Mouchot, M. C. (1992) 'Use of satellite imagery in management of giant kelp resources, Morbihan Gulf, Kerguelen archipelago', *Oceanologica Acta*, 15(3), pp. 297–307.

Bennion, M. *et al.* (2019) 'Remote Sensing of Kelp (Laminariales, Ochrophyta): Monitoring Tools and Implications for Wild Harvesting', *Reviews in Fisheries Science & Aquaculture*, 27(2), pp. 127–141. doi: 10.1080/23308249.2018.1509056.

Bivand, R., Keitt, T. and Rowlingson, B. (2020) 'rgdal: Bindings for the "Geospatial" Data Abstraction Library.R package version 1.5-15.' Available at: https://cran.r-project.org/package=rgdal.

Bivand, R. and Lewin-Koh, N. (2020) 'maptools: Tools for Handling Spatial Objects. R package version 1.0-1.' Available at: https://cran.r-project.org/package=maptools.

Bolton, J. J. (2010) 'The biogeography of kelps (Laminariales, Phaeophyceae): A global analysis with new insights from recent advances in molecular phylogenetics', *Helgoland Marine Research*. BioMed Central, 64(4), pp. 263–279. doi: 10.1007/s10152-010-0211-6.

Breeman, A. M. (1988) 'Relative importance of temperature and other factors in determining geographic boundaries of seaweeds: experimental and phenological evidence*', *Helgolander Meeresuntersuchungen* , 42, pp. 99–241.

British Geological Survey (2011) *DiGSBS250K [SHAPE geospatial data], Scale 1:250000, Tiles: GB*, *EDINA Geology Digimap Service*. Available at: https://digimap.edina.ac.uk (Accessed: 28 April 2020).

Brodie, J. *et al.* (2014) 'The future of the northeast Atlantic benthic flora in a high CO_2 world', *Ecology and Evolution*. John Wiley and Sons Ltd, 4(13), pp. 2787–2798. doi: 10.1002/ece3.1105.

Brodie, J. *et al.* (2018) 'A comparison of multispectral aerial and satellite imagery for mapping intertidal seaweed communities', *Aquatic Conservation: Marine and Freshwater Ecosystems*. John Wiley and Sons Ltd, 28(4), pp. 872–881. doi: 10.1002/aqc.2905.

Brooks, T. M. *et al.* (2002) 'Habitat loss and extinction in the hotspots of biodiversity', *Conservation Biology*. John Wiley & Sons, Ltd, 16(4), pp. 909–923. doi: 10.1046/j.1523-1739.2002.00530.x.

Bruckner, C. T. and Yoder, P. (2006) 'Interpreting kappa in observational research: Baserate matters', *American Journal on Mental Retardation*. Allen Press, 111(6), pp. 433–441. doi: 10.1352/0895-8017(2006)111[433:IKIORB]2.0.CO;2.

Brunsdon, C. and Chen, H. (2014) 'GISTools: Some further GIS capabilities for R. R package version 0.7-4'. Available at: https://cran.r-project.org/package=GISTools.

Casal, G., Kutser, T., *et al.* (2011) 'Mapping benthic macroalgal communities in the coastal zone using CHRIS-PROBA mode 2 images', *Estuarine, Coastal and Shelf Science*. Academic Press, 94(3), pp. 281–290. doi: 10.1016/j.ecss.2011.07.008.

Casal, G., Sánchez-Carnero, N., *et al.* (2011) 'Remote sensing with SPOT-4 for mapping kelp forests in turbid waters on the south European Atlantic shelf', *Estuarine, Coastal and Shelf Science*. Academic Press, 91(3), pp. 371–378. doi: 10.1016/j.ecss.2010.10.024.

Chimet Support Group (2020) *Chimet, weather reports from Chichester Bar*. Available at: https://www.chimet.co.uk/(S(svsu2345fqswwfbyc0fpd545))/Default.aspx (Accessed: 28 April 2020).

Christie, H., Fredriksen, S. and Rinde, E. (1998) 'Regrowth of kelp and colonization of epiphyte and fauna community after kelp trawling at the coast of norway', in *Hydrobiologia*. Springer Netherlands, pp. 49–58. doi: 10.1007/978-94-017-2864-5_4.

Christie, H., Norderhaug, K. and Fredriksen, S. (2009) 'Macrophytes as habitat for fauna', *Marine Ecology Progress Series*, 396, pp. 221–233. doi: 10.3354/meps08351.

Chung, I. K. *et al.* (2011) 'Using marine macroalgae for carbon sequestration: A critical appraisal', *Journal of Applied Phycology*. Springer, 23(5), pp. 877–886. doi: 10.1007/s10811-010-9604-9.

Cohen, J. (1960) 'A Coefficient of Agreement for Nominal Scales', *Educational and Psychological Measurement*. Sage PublicationsSage CA: Thousand Oaks, CA, 20(1), pp. 37–46. doi: 10.1177/001316446002000104.

Convention on Biological Diversity (2018) *Aichi Biodiversity Targets*. Secretariat of the Convention on Biological Diversity. Available at: https://www.cbd.int/sp/targets/ (Accessed: 12 August 2020).

Davies, D. and Nelson, K. (2019) *Centuries of Sussex Seas A summary of historic fishing activity in Sussex coastal waters, report for Sussex IFCA*.

Dayton, P. K. (1985) 'Ecology of Kelp Communities', *Annual Review of Ecology and Systematics*, 16, pp. 215–245.

Dayton, P. K. *et al.* (1992) 'Temporal and Spatial Patterns of Disturbance and Recovery in a Kelp Forest Community', *Ecological Monographs*. Ecological Society of America, 62(3), pp. 421–445.

555 doi: 10.2307/2937118.

556 Desgraupes, B. (2018) ‘clusterCrit: Clustering Indices. R package version 1.2.8.’ Available at:
557 https://cran.r-project.org/package=clusterCrit.

558 Deysher, L. E. (1993) *Evaluation of remote sensing techniques for monitoring giant kelp*
559 *populations 307*, *Hydrobiologia*.

560 Dowle, M. and Srinivasan, A. (2020) ‘data.table: Extension of `data.frame`. R package version
561 1.13.0’. Available at: https://cran.r-project.org/web/packages/data.table/index.html.

562 Dunnington, D. (2020) ‘ggspatial: Spatial Data Framework for ggplot2. R package version 1.1.4’.
563 Available at: https://cran.r-project.org/package=ggspatial.

564 European Space Agency (2015) *Sentinel-2 User Handbook*. Available at:
565 https://earth.esa.int/documents/247904/685211/Sentinel-2_User_Handbook (Accessed: 5 August
566 2020).

567 European Space Agency (2020a) *Copernicus Open Access Hub*. Available at:
568 https://scihub.copernicus.eu/dhus/#/home (Accessed: 5 August 2020).

569 European Space Agency (2020b) *Radiometric Resolutions, Sentinel-2 MSI*. Available at:
570 https://sentinel.esa.int/web/sentinel/user-guides/sentinel-2-msi/resolutions/radiometric (Accessed:
571 5 August 2020).

572 Fahrig, L. (1997) ‘Relative Effects of Habitat Loss and Fragmentation on Population Extinction’,
573 *The Journal of Wildlife Management*. JSTOR, 61(3), p. 603. doi: 10.2307/3802168.

574 FAO (2018) *The global status of seaweed production, trade and utilization Volume 124*. Rome.

575 Garcia, C. and Sitjar, J. (2020) *Script to monitor aquatic plants and algae using satellite images*.
576 Available at: https://www.unigis.es/script-para-monitorizar-la-presencia-de-plantas-acuaticas-y-
577 algas-mediante-imagenes-satelite/ (Accessed: 2 June 2020).

578 Global Fishing Watch (2020) *How our vessel tracking map works*. Available at:
579 https://globalfishingwatch.org/map-and-data/technology/ (Accessed: 24 August 2020).

580 Greenberg, J. A. and Mattiuzzi, M. (2020) ‘gdalUtils: Wrappers for the Geospatial Data Abstraction
581 Library (GDAL) Utilities. R package version 2.0.3.2.’ Available at:
582 https://cran.rproject.org/package=gdalUtils.

583 Guillaumont, B., Callens, L. and Dion, P. (1993) ‘Spatial distribution and quantification of Fucus
584 species and Ascophyllum nodosum beds in intertidal zones using spot imagery’, *Hydrobiologia*.
585 Kluwer Academic Publishers, 260–261(1), pp. 297–305. doi: 10.1007/BF00049032.

586 Hijmans, R. J. (2019) ‘geosphere: Spherical Trigonometry. R package version 1.5-10.’ Available at:

https://cran.r-project.org/package=geosphere.

Hijmans, R. J. (2020) ‘raster: Geographic Data Analysis and Modeling. R package version 3.3-13’. Available at: https://cran.r-project.org/package=raster.

Hiscock, K. (1996) *SACFOR aMarine Nature Conservation Review: Rationale and methods. Coasts and seas of the United Kingdom. MNCR series*. Peterborough: Joint Nature Conservation Committee.

Hiscock, K. *et al.* (2004) ‘Effects of changing temperature on benthic marine life in Britain and Ireland’, *Aquatic Conservation: Marine and Freshwater Ecosystems*. John Wiley & Sons, Ltd, 14(4), pp. 333–362. doi: 10.1002/aqc.628.

Holmes, I. (2017) *Mean High Water Springs Polygon, [Dataset].*, *University of Edinburgh*. Available at: https://doi.org/10.7488/ds/1969 (Accessed: 22 April 2020).

Hu, C. (2009) ‘A novel ocean color index to detect floating algae in the global oceans’, *Remote Sensing of Environment*. Elsevier, 113(10), pp. 2118–2129. doi: 10.1016/j.rse.2009.05.012.

International Union for Conservation of Nature (2020) *Red List of Ecosystems*. Available at: https://www.iucn.org/theme/ecosystem-management/our-work/red-list-ecosystems (Accessed: 12 August 2020).

James, D. and Hornik, K. (2020) ‘chron: Chronological Objects which Can Handle Dates and Times. R package version 2.3-55.’ Available at: https://rdrr.io/cran/chron/.

Jensen, J. R., Estes, J. E. and Tinney, L. (1980) ‘Remote Sensing Techniques for Kelp Surveys’, *Photogrammetric Engineering and Remote Sensing*, 46(6), pp. 743–755.

Kaufman, L. and Rousseeuw, P. J. (1990) ‘Clustering Large Applications (Program CLARA)’, in Kaufman, L. and Rousseeuw, P. J. (eds) *Finding Groups in Data*. New Jersey: John Wiley & Sons, Ltd, pp. 126–163. doi: 10.1002/9780470316801.ch3.

Kellaris, A. *et al.* (2019) ‘Using low-cost drones to monitor heterogeneous submerged seaweed habitats: A case study in the Azores’, *Aquatic Conservation: Marine and Freshwater Ecosystems*. John Wiley and Sons Ltd, 29(11), pp. 1909–1922. doi: 10.1002/aqc.3189.

Kelley, T. L. (1935) ‘An Unbiased Correlation Ratio Measure’, *Proceedings of the National Academy of Sciences*. Proceedings of the National Academy of Sciences, 21(9), pp. 554–559. doi: 10.1073/pnas.21.9.554.

Kirk, J. T. O. (1994) *Light and Photosynthesis in Aquatic Ecosystems*. 2nd edn. Cambridge: Cambridge University Press.

Kutser, T., Vahtmäe, E. and Martin, G. (2006) ‘Assessing suitability of multispectral satellites for mapping benthic macroalgal cover in turbid coastal waters by means of model simulations’,

Estuarine, Coastal and Shelf Science. Academic Press, 67(3), pp. 521–529. doi: 10.1016/j.ecss.2005.12.004.

Lüdecke *et al.* (2020) 'Assessment of Regression Models Performance. CRAN.' Available at: https://rdrr.io/cran/performance/.

Lüdecke, D. (2020) 'sjPlot: Data Visualization for Statistics in Social Science. R package version 2.8.4'. Available at: https://cran.r-project.org/package=sjPlot.

Lyzenga, D. R. (1978) 'Passive remote sensing techniques for mapping water depth and bottom features', *Applied Optics*. The Optical Society, 17(3), p. 379. doi: 10.1364/ao.17.000379.

Lyzenga, D. R. (1981) 'Remote sensing of bottom reflectance and water attenuation parameters in shallow water using aircraft and landsat data', *International Journal of Remote Sensing*. Taylor & Francis Group , 2(1), pp. 71–82. doi: 10.1080/01431168108948342.

MacQueen, J. (1967) 'Some Methods for Classification and Analysis of Multivariate Observations', in *Proceedings of the Fifth Berkeley Symposium on Mathematical Statistics and Probability*. Volume 1: Berkeley, California: University of California Press, pp. 281–97.

Maechler, M. *et al.* (2019) 'cluster: Cluster Analysis Basics and Extensions. R package version 2.1.0.'. Available at: https://cran.r-project.org/web/packages/cluster/index.html.

Mahmoudian, M. (2020) 'varhandle: Functions for Robust Variable Handling. R package version 2.0.5.' Available at: https://cran.r-project.org/package=varhandle.

Mangiafico, S. (2020) 'rcompanion: Functions to Support Extension Education Program Evaluation. R package version 2.3.25.' Available at: https://cran.r-project.org/package=rcompanion.

McHugh, M. L. (2012) 'Interrater reliability: The kappa statistic', *Biochemia Medica*. Biochemia Medica, Editorial Office, 22(3), pp. 276–282. doi: 10.11613/bm.2012.031.

Meyer, D. *et al.* (2019) 'e1071: Misc Functions of the Department of Statistics, Probability Theory Group (Formerly: E1071), TU Wien. R package version 1.7-3.' Available at: https://cran.r-project.org/package=e1071.

Mac Monagail, M. *et al.* (2017) 'Sustainable harvesting of wild seaweed resources', *European Journal of Phycology*. Taylor and Francis Ltd., 52(4), pp. 371–390. doi: 10.1080/09670262.2017.1365273.

Mora-Soto, A. *et al.* (2020) 'A High-Resolution Global Map of Giant Kelp (Macrocystis pyrifera) Forests and Intertidal Green Algae (Ulvophyceae) with Sentinel-2 Imagery', *Remote Sensing*. Multidisciplinary Digital Publishing Institute, 12(4), p. 694. doi: 10.3390/rs12040694.

National Biodiversity Network Atlas (2020) *Occurrence records*. Available at: https://records.nbnatlas.org/occurrences/search?q=*%3A*&fq=(taxon_name%3A%22Laminaria

653 digitata%22 OR taxon_name%3A%22Laminaria hyperborea%22 OR
654 taxon_name%3A%22Saccharina latissima%22)&wkt=MULTIPOLYGON(((-0.8481279015541076
655 50.84322382170522%2C-0.84812790 (Accessed: 10 August 2020).

656 Neuwirth, E. (2014) 'RColorBrewer: ColorBrewer Palettes. R package version 1.1-2'. Available at:
657 https://cran.r-project.org/package=RColorBrewer.

658 OceanWise (2016) *Marine Themes Digital Elevation Model 1 Arc Second [ASC geospatial data],*
659 *Scale 1:50000*, *EDINA Marine Digimap Service*. Available at: https://digimap.edina.ac.uk
660 (Accessed: 28 April 2020).

661 Pardini, R., Nichols, E. and Püttker, T. (2017) 'Biodiversity response to habitat loss and
662 fragmentation', in DellaSala, D. and Goldstein, M. (eds) *Encyclopedia of the Anthropocene*.
663 Amsterdam: Elsevier, pp. 229–239. doi: 10.1016/B978-0-12-809665-9.09824-4.

664 Pebesma, E. (2018) 'Simple Features for R: Standardized Support for Spatial Vector Data.', *The R*
665 *Journal*, 10(1), pp. 439–446.

666 Pebesma, E. J. and Bivand, R. S. (2005) 'Classes and methods for spatial data in R.', *R News*,
667 5(2).

668 Pessarrodona, A. *et al.* (2018) 'Carbon assimilation and transfer through kelp forests in the NE
669 Atlantic is diminished under a warmer ocean climate', *Global Change Biology*. Blackwell Publishing
670 Ltd, 24(9), pp. 4386–4398. doi: 10.1111/gcb.14303.

671 Pettorelli, N., Safi, K. and Turner, W. (2014) 'Satellite remote sensing, biodiversity research and
672 conservation of the future', *Philosophical Transactions of the Royal Society B: Biological Sciences*.
673 Royal Society, 369(1643), p. 20130190. doi: 10.1098/rstb.2013.0190.

674 QGIS Development Team (2020) 'QGIS Geographic Information System'. Open Source Geospatial
675 Foundation Project. Available at: http://qgis.org.

676 R Core Team (2019) 'R: A language and environment for statistical computing'. Vienna, Austria: R
677 Foundation for Statistical Computing. Available at: https://www.r-project.org/.

678 Ross, N. (2020) 'fasterize: Fast Polygon to Raster Conversion. R package version 1.0.3'. Available
679 at: https://cran.r-project.org/package=fasterize.

680 RStudio Team (2020) 'RStudio: Integrated Development for R'. Boston, MA: RStudio, PBC.
681 Available at: http://www.rstudio.com/.

682 Sagawa, T. *et al.* (2010) 'Using bottom surface reflectance to map coastal marine areas: a new
683 application method for Lyzenga's model', *International Journal of Remote Sensing*. Taylor and
684 Francis Ltd., 31(12), pp. 3051–3064. doi: 10.1080/01431160903154341.

685 Schoener, T. W. (1970) 'Nonsynchronous spatial overlap of lizards in patchy habitats', *Ecology*, 51,

pp. 408–418.

Seasearch (2019) *Seasearch Marine Surveys in England, accessed through NBN Atlas website.* doi: 10.15468/kywx6m.

Slowikowski, K. (2020) 'ggrepel: Automatically Position Non-Overlapping Text Labels with "ggplot2". R package version 0.8.2'.

Smale, D. A. *et al.* (2013) 'Threats and knowledge gaps for ecosystem services provided by kelp forests: A northeast Atlantic perspective', *Ecology and Evolution*. John Wiley & Sons, Ltd, 3(11), pp. 4016–4038. doi: 10.1002/ece3.774.

Smith, C. J. *et al.* (2003) 'Analysing the impact of bottom trawls on sedimentary seabeds with sediment profile imagery', *Journal of Experimental Marine Biology and Ecology*. Elsevier, 285–286, pp. 479–496. doi: 10.1016/S0022-0981(02)00545-2.

Steen, H. *et al.* (2016) 'Regrowth after kelp harvesting in Nord-Trøndelag, Norway', *ICES Journal of Marine Science: Journal du Conseil*. Oxford University Press (OUP), 73(10), pp. 2708–2720. doi: 10.1093/icesjms/fsw130.

Steneck, R. S. *et al.* (2002) 'Kelp forest ecosystems: biodiversity, stability, resilience and future Kelp forest ecosystems', *Environmental Conservation*, 29(4), pp. 436–459. doi: 10.1017/S0376892902000322.

Sussex Inshore Fisheries and Conservation Authority (2020) *Kelp*. Available at: https://www.sussex-ifca.gov.uk/kelp (Accessed: 1 March 2020).

Teagle, H. *et al.* (2017) 'The role of kelp species as biogenic habitat formers in coastal marine ecosystems', *Journal of Experimental Marine Biology and Ecology*. Elsevier B.V., pp. 81–98. doi: 10.1016/j.jembe.2017.01.017.

Tides4Fishing (2020) *Tide times and charts for Selsey Bill, England and weather forecast for Selsey Bill*. Available at: https://tides4fishing.com/uk/england/selsey-bill (Accessed: 26 April 2020).

Turner, W. *et al.* (2003) 'Remote sensing for biodiversity science and conservation', *Trends in Ecology and Evolution*. Elsevier Ltd, pp. 306–314. doi: 10.1016/S0169-5347(03)00070-3.

Volent, Z., Johnsen, G. and Sigernes, F. (2007) 'Kelp forest mapping by use of airborne hyperspectral imager', *Journal of Applied Remote Sensing*. SPIE-Intl Soc Optical Eng, 1(1), p. 011503. doi: 10.1117/1.2822611.

Van der Wal, D. *et al.* (2014) 'Biophysical control of intertidal benthic macroalgae revealed by high-frequency multispectral camera images', *Journal of Sea Research*. Elsevier, 90, pp. 111–120. doi: 10.1016/j.seares.2014.03.009.

Wickham, H. (2016) *ggplot2: Elegant Graphics for Data Analysis*. New York: Springer-Verlag.

Wickham, H. *et al.* (2020) ‘dplyr: A Grammar of Data Manipulation. R package version 1.0.1.’ Available at: https://cran.r-project.org/package=dplyr.

Wickham, H. and Henry, L. (2020) ‘tidyr: Tidy Messy Data. R package version 1.1.0.’ Available at: https://cran.r-project.org/package=tidyr.

Williams, C. and Davies, W. (2019) *Valuing the ecosystem service benefits of kelp bed recovery off West Sussex, report for Sussex IFCA.* Available at: www.nefconsulting.com (Accessed: 2 March 2020).

Wilmers, C. C. *et al.* (2012) ‘Do trophic cascades affect the storage and flux of atmospheric carbon? An analysis of sea otters and kelp forests’, *Frontiers in Ecology and the Environment*. John Wiley & Sons, Ltd, 10(8), pp. 409–415. doi: 10.1890/110176.

Xie, Y. (2020) ‘knitr: A General-Purpose Package for Dynamic Report Generation in R. R package version 1.29.’

Yesson *et al.* (2015a) ‘Large brown seaweeds of the british isles: Evidence of changes in abundance over four decades’, *Estuarine, Coastal and Shelf Science*. doi: 10.1016/j.ecss.2015.01.008.

Yesson *et al.* (2015b) ‘The distribution and environmental requirements of large brown seaweeds in the British Isles’. doi: 10.1017/S0025315414001453.

Yesson, C., Ash, L. and Brodie, J. (2015) *Using aerial images to quantify the extent of coastal seaweed habitats*. London, United Kingdom.

Zeileis, A. and Hothorn, T. (2002) ‘Diagnostic Checking in Regression Relationships’, *R News*, 2(3), pp. 7–10. Available at: https://cran.r-project.org/doc/Rnews/.

Zeileis, A., Kleiber, C. and Jackman, S. (2008) ‘Regression Models for Count Data in R.’, *Journal of Statistical Software*, 27(8).

Zoffoli, M. L., Frouin, R. and Kampel, M. (2014) ‘Water column correction for coral reef studies by remote sensing’, *Sensors (Switzerland)*. MDPI AG, pp. 16881–16931. doi: 10.3390/s140916881.

Supplementary Information

Supplementary Information 1

Table 1: Wavelength and bandwidth specifications for each spectral band of Sentinel L2a satellite imagery used for this study. Adapted from European Space Agency (2020b).

Band	Name	Central wavelength (nm)	Bandwidth (nm)
10m resolution			
2	Blue	492.4	66
3	Green	559.8	36
4	Red	664.6	31
8	Near Infra-Red	832.8	106
20m resolution			
5	VNIR vegetation red edge spectral domain	704.1	15
6		740.5	15
7		782.8	20
8a		864.7	21
11	SWIR bands	1613.7	91
12		2202.4	175

Supplementary Information 2

Table 1: Metadata for all available satellite imagery collected by the Sentinel satellite constellation for the study area, not obscured by cloud (European Space Agency, 2020a). Tidal and weather condition data were used to select images for seabed classification with minimal water depth, turbidity, and suspended sediment.

Satellite image collection date	Time (GMT)	Avg. cloud cover (%)	Closest high tide	Closest low tide	Water depth (m)	Avg. windspeed (knots)		Avg. wave height (m)	
						Collection day	*Prior day*	*Collection day*	*Prior day*
20/07/20	11:06	26.93	11:42	05:16	4.7	13.26	6.28	0.07	0.12
21/04/20	11:06	3.62	10:27	16:26	4.8	16.13	20.00	0.36	0.22
11/04/20	11:06	4.70	13:15	07:10	4.3	12.31	14.45	0.19	0.20
26/02/19	11:10	0.09	15:07	08:40	2.0	8.85	7.97	0.75	0.72
09/10/18	11:09	0.96	10:58	17:18	5.5	11.37	9.92	0.27	0.18
26/06/18	11:06	0.24	09:59	16:03	4.6	5.15	6.23	0.07	0.09
22/04/18	11:06	4.34	15:37	09:00	1.7	5.48	9.84	0.20	0.26

Supplementary Information 3

20.07.20 image

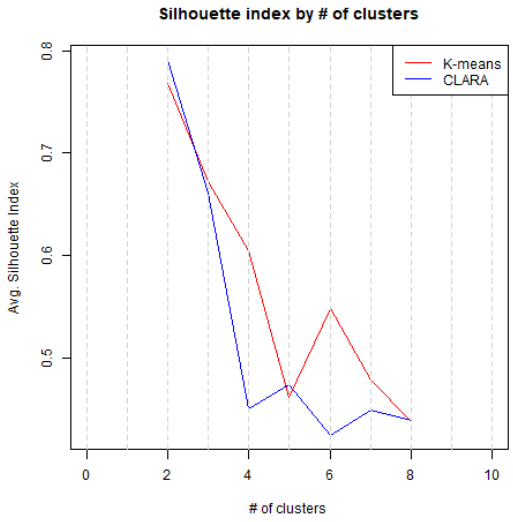

21.04.20 image

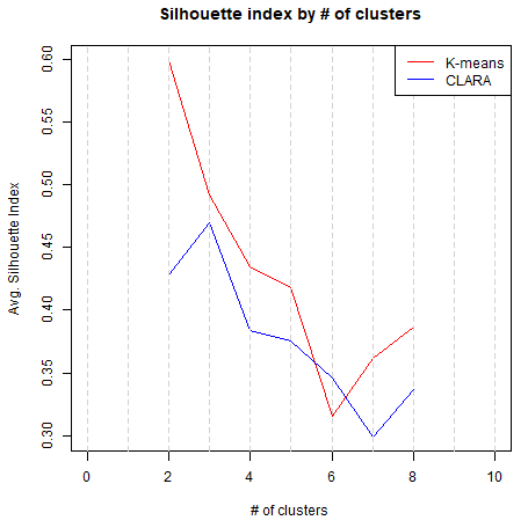

26.02.19 image

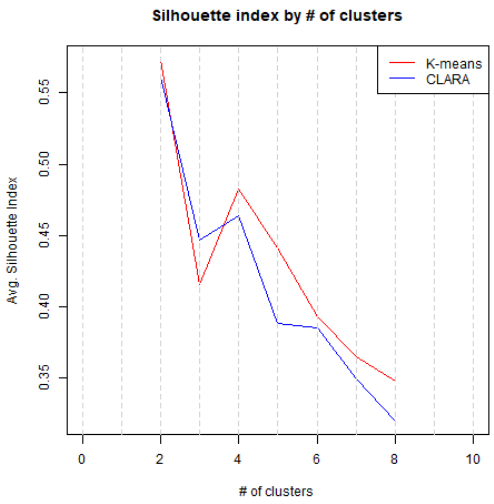

22.04.18 image

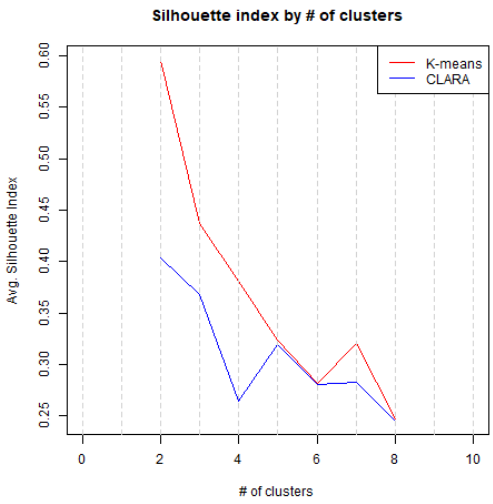

Figure 1: Graphs showing the similarity of observations to their clusters (silhouette index) for K-means and CLARA clustering algorithms used to perform unsupervised image classification. The algorithms were run on 2-8 clusters and the silhouette index used to select the most appropriate clustering method and number of clusters for each image.

Supplementary Information 4

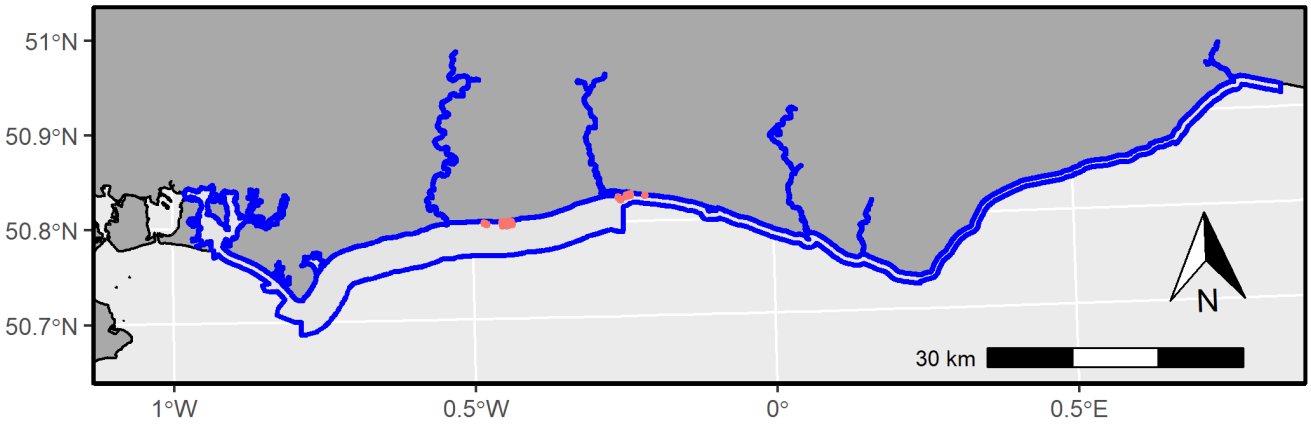

Figure 1: Map of bare sand points along the Sussex coast, identified using geology data and satellite imagery, used to carry out water attenuation correction. The blue line indicates the area where trawling will be banned to protect kelp (*Laminaria* spp.).

Supplementary Information 5

Table 1: Coefficients for multiple linear regressions showing the rate of light attenuation through the water column (attenuation coefficients) at varying depths. Logged values for each light band are taken as the response variables for each model, and depth as the explanatory variable.

Log near infra-red band

Predictors	*Estimates*	*CI*	*p*
(Intercept)	9.44	7.74 – 11.15	<**0.001**
Depth	-0.85	-1.20 – -0.49	<**0.001**
Observations	20		
R^2 / R^2 adjusted	0.58 / 0.56		

Log red band

Predictors	*Estimates*	*CI*	*p*
(Intercept)	9.69	8.61 – 10.78	<**0.001**
Depth	-0.68	-0.90 – -0.45	<**0.001**
Observations	20		
R^2 / R^2 adjusted	0.69 / 0.67		

Log green band

Predictors	*Estimates*	*CI*	*p*
(Intercept)	8.77	8.10 – 9.45	<**0.001**
Depth	-0.36	-0.51 – -0.22	<**0.001**
Observations	20		
R^2 / R^2 adjusted	0.62 / 0.60		

Log blue band

Predictors	*Estimates*	*CI*	*p*
(Intercept)	8.41	7.67 – 9.15	<**0.001**
Depth	-0.35	-0.51 – -0.20	<**0.001**
Observations	20		
R^2 / R^2 adjusted	0.57 / 0.54		

Supplementary Information 6

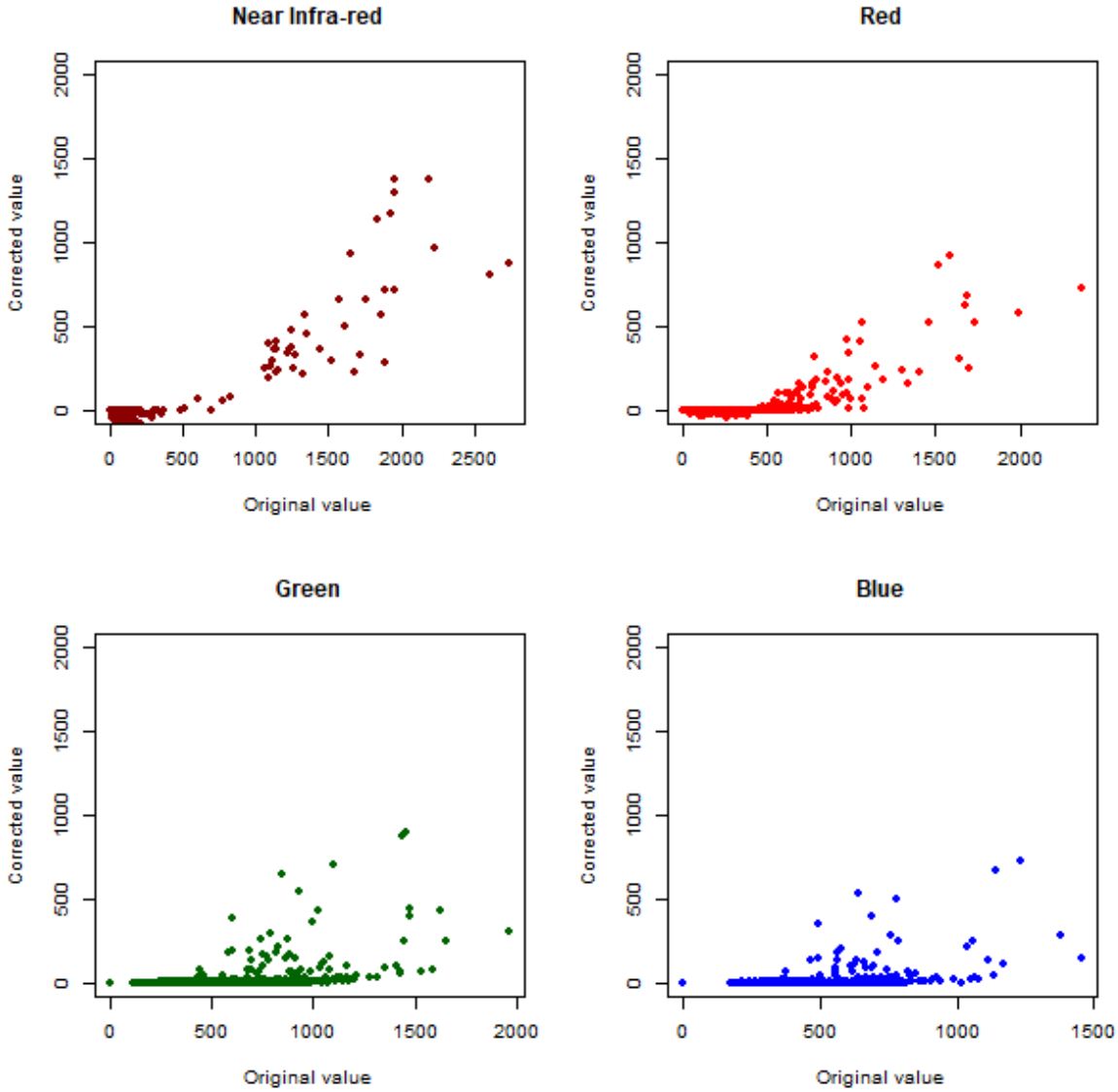

Figure 1: Scatter plots showing reflectance values collected by satellite imagery for each spectral band, compared to values corrected for light attenuation within the water column.

Supplementary Information 7

Table 1: Pairwise comparisons of predicted habitat class (kelp presence/absence) between seabed sediment classes, using Mann-Whitney U test. Adjusted p values using "fdr" control the false discovery rate (expected proportion of false positives), less stringently than family-wise error therefore having a higher power for large datasets.

	Gravelly muddy sand	**Gravel**	**Gravelly sand**	**Muddy sandy gravel**	**Muddy sand**	**Sandy gravel**	**Sandy mud**	**Slightly gravelly muddy sand**	**Slightly gravelly sand**	**Slightly gravelly sandy mud**	**Sand**	**Rock**
Gravel	<0.001	-	-	-	-	-	-	-	-	-	-	-
Gravelly sand	<0.001	<0.001	-	-	-	-	-	-	-	-	-	-
Muddy sandy gravel	0.3203	<0.001	<0.001	-	-	-	-	-	-	-	-	-
Muddy sand	<0.001	<0.001	<0.001	<0.001	-	-	-	-	-	-	-	-
Sandy gravel	<0.001	<0.001	<0.001	<0.001	<0.001	-	-	-	-	-	-	-
Sandy mud	<0.001	<0.001	<0.001	<0.001	<0.001	<0.001	-	-	-	-	-	-
Slightly gravelly muddy sand	<0.001	<0.001	<0.001	<0.001	<0.001	<0.001	<0.001	-	-	-	-	-
Slightly gravelly sand	<0.001	<0.001	<0.001	<0.001	<0.001	<0.001	<0.001	<0.001	-	-	-	-
Slightly gravelly sandy mud	<0.001	<0.001	<0.001	<0.001	<0.001	<0.001	<0.001	<0.001	<0.001	-	-	-
Sand	<0.001	<0.001	<0.001	<0.001	<0.001	<0.001	<0.001	<0.001	<0.001	<0.001	-	-
Rock	<0.001	<0.001	<0.001	<0.001	<0.001	<0.001	<0.01	<0.001	<0.001	<0.001	<0.001	-
Rock and sediment	<0.001	<0.001	<0.001	<0.001	<0.001	<0.001	<0.001	<0.001	<0.001	0.21	<0.001	<0.001